Adiabatic magnetocaloric effect in $Ni_{50}Mn_{35}In_{15}$ ribbons

P. Álvarez-Alonso, C. O. Aguilar-Ortiz, J. P. Camarillo, D. Salazar, H. Flores-Zúñiga, and V. A. Chernenko

Citation: Appl. Phys. Lett. **109**, 212402 (2016); doi: 10.1063/1.4968592
View online: https://doi.org/10.1063/1.4968592
View Table of Contents: http://aip.scitation.org/toc/apl/109/21
Published by the American Institute of Physics

Adiabatic magnetocaloric effect in $Ni_{50}Mn_{35}In_{15}$ ribbons

P. Álvarez-Alonso,[1,a)] C. O. Aguilar-Ortiz,[2] J. P. Camarillo,[2] D. Salazar,[3] H. Flores-Zúñiga,[2] and V. A. Chernenko[1,3,4]
[1]*Departamento de Electricidad y Electrónica, Universidad del País Vasco (UPV/EHU), 48940 Leioa, Spain*
[2]*División de Materiales Avanzados, IPICYT, 78216 San Luis Potosí, Mexico*
[3]*BCMaterials, Bizkaia Science and Technology Park, Derio 48160, Spain*
[4]*Ikerbasque, Basque Foundation for Science, 48013 Bilbao, Spain*

(Received 3 October 2016; accepted 6 November 2016; published online 22 November 2016)

Heusler-type Ni-Mn-based metamagnetic shape memory alloys (MetaMSMAs) are promising candidates for magnetic refrigeration. To increase heat exchange rate and efficiency of cooling, the material should have a high surface/volume ratio. In this work, the typical $Ni_{50}Mn_{35}In_{15}$ MetaMSMA was selected to fabricate thin ribbons by melt-spinning. The characteristic transformations of the ribbons were determined by calorimetry, X-ray diffraction, scanning electron microscopy and thermomagnetization measurements. The inverse and conventional magnetocaloric effects (MCEs) associated with the martensitic transformation (MT) and the ferromagnetic transition of the austenite (T_C^A), respectively, were measured directly by the adiabatic method (ΔT_{ad}) and indirectly by estimating the magnetic entropy change from magnetization measurements. It is found that the ribbons exhibit large values of $\Delta T_{ad} = -1.1$ K at $\mu_0 \Delta H = 1.9$ T, in the vicinity of the MT temperature of 300 K for inverse MCE, and $\Delta T_{ad} = 2.3$ K for conventional MCE at $T_C^A = 309$ K. This result strongly motivates further development of different MetaMSMA refrigerants shaped as ribbons. *Published by AIP Publishing*. [http://dx.doi.org/10.1063/1.4968592]

Magnetic refrigeration (MR), a solid state technology based on the magnetocaloric effect (MCE), has attracted great interest because of several environmental advantages (for instance, its larger energy efficiency) compared with the traditional cooling systems.[1,2] Among the candidates as magnetic coolants for MR at room temperature, the Ni-Mn-based Heusler alloys, a family of metamagnetic shape memory alloys (MetaMSMAs), are outstanding materials because (i) they can exhibit abrupt changes in their magnetic properties induced by a magnetostructural transition from the weakly magnetic martensite to a ferromagnetic austenite, which is usually associated with giant inverse MCE (i.e., with the opposite sign compared with conventional magnetocaloric),[3] and (ii) the martensitic transformation (MT) temperatures can be easily tuned in a wide temperature range including the room temperature by slight changes in the composition, since they are highly dependent on the valence electron concentration per atom e/a.[4]

Aside from investigating new materials with enlarged magnetocaloric responses, a growing research field consists of finding new performance optimization methods of MR systems; in particular, it has recently been stressed that thermal inertia must be minimized in magnetic coolants by allowing the increase in cycling frequencies and cooling power of refrigerant systems.[5,6] In this sense, the use of materials with reduced dimensions results in a propitious approach to decrease the thermal inertia.[7,8] Melt-spinning is a well-established technique for processing materials presenting MCE in ribbon form with typical thicknesses of around 20–40 μm. Besides, the previous works on MetaMSMAs have demonstrated the large capabilities of this method to modify MT temperatures and magnetic and transport properties of the parent bulk alloys, including their magnetocaloric response.[5] However, due to the inherent difficulties with the measurements of the adiabatic temperature changes arising from the low thermal mass of small samples, the vast majority of works on the MCE materials with the micrometer-scale dimensions have been exclusively dealing with the isothermal magnetic entropy change, ΔS_M, estimated from magnetization measurements.[2] Incidentally, one should emphasize that most of the known-to-date room-temperature refrigerator prototypes are based on the active magnetic regenerator and Brayton thermodynamic cycles, where the refrigerant undergoes two adiabatic magnetization-demagnetization processes.[9] In fact, only few reports about the direct adiabatic measurements of MCE in ribbons can be found in the literature. Such measurements have been carried out for amorphous Fe-based alloys[11,12] and Gd-Co-Al[13] (both exhibit a second-order transition), and for $Ni_{50}Mn_{37}Sn_{13}$ MetaMSMA. The last ribbon showed a very small value of ΔT_{ad} due to the low magnetic field applied, $\mu_0 \Delta H < 0.06$ T.[10]

Taking into account the lack of ΔT_{ad} data in MetaMSMA ribbons and their importance for MR, we have recently designed and built-up a sensitive set-up for adiabatic measurements at different constant temperatures under magnetic fields up to 1.9 T. For these measurements, in this work, we have fabricated the ribbons of a well-studied $Ni_{50}Mn_{35}In_{15}$ MetaMSMA exhibiting MT close to room temperature. The measurements demonstrated the inspiring values of ΔT_{ad} in the ribbons, which are consistent with the adiabatic data reported in the literature on a bulk alloy of the same composition. For the sake of completeness, we also acquired the thermomagnetic behavior of the ribbons and calculated magnetic entropy change.

Polycrystalline master alloy was prepared from pure elements by arc melting in an Ar atmosphere and re-melted

a)Author to whom correspondence should be addressed. Electronic mail: alvarez.alonso.pablo@gmail.com

several times to ensure the homogeneity of the ingot. The melt-spun ribbons (flakes of 50 μm thick and 1.2 mm wide) with a nominal composition of $Ni_{50}Mn_{35}In_{15}$ (at. %) were produced by melt spinning with a surface velocity of 10 ms^{-1}. A Hitachi TM3000 Scanning Electron Microscope (SEM) equipped with an X-ray energy dispersive spectroscopy (EDS) system and a cryothermostat were used to examine the microstructure and chemical composition of the ribbons. The composition of the melt-spun ribbons was $Ni_{50.7}Mn_{35.2}In_{14.1}$, close to the nominal. Differential scanning calorimetry (DSC) analysis was performed by a TA-Instruments Q200 calorimeter with a temperature rate of 10 K/min. The characteristic MT temperatures, T_{ms}, T_{mf}, T_{as}, and T_{af}, were determined from the DSC peaks by a standard tangent method.[14] An X-ray powder diffraction pattern was collected at 350 K in a Bruker D8 Advance Vantec diffractometer with Cu-Kα radiation using powdered samples to avoid the influence of texture. The analysis of the diffraction pattern was performed using the FullProf Suite.[15] Magnetization measurements were carried out in a magnetic measurement platform (CFMS, Cryogenic Ltd.) equipped with a vibrating sample magnetometer. To reduce the effect of the demagnetizing field, ribbons were aligned with the magnetic field. Magnetic entropy change was estimated from the $M(T)$ curves at different applied magnetic fields using a well-known Maxwell relationship.[16]

The field-induced adiabatic temperature change was measured by a specially designed set-up,[17] enabling a maximum field of 1.9 T with large field change rates of ~2 T/s. The sample represented a pack of the several ribbons assembled in a good thermal contact between them. The sample temperature was monitored with an accuracy better than 0.02 K by a type-T (copper-constantan) thermocouple with a diameter of ~80 μm tightly fixed inside the package to reduce thermal losses. To avoid spurious effects due to the MT thermal hysteresis, ΔT_{ad} was measured following a specific thermal protocol: first, the temperature of the specimen was set to 15 K below (above) T_{as} (T_{ms}) when heating (cooling); second, the sample was heated (cooled) to the target measuring temperature (with maximum overheat/overcool of 0.05 K at its approach); and then, the magnetic field is applied. When the magnetic field is removed, the protocol starts again from the first step to ensure the initial transformation volume fraction in the sample.

Figure 1(a) depicts the DSC cooling/heating curves of the Ni-Mn-In ribbon, which present large exothermic and endothermic anomalies with moderate thermal hysteresis (signatures of a first-order phase transition) corresponding to the forward (upon cooling) and reverse (upon heating) MT, respectively. The DSC cooling ramp presents small shoulder (indicated by a vertical arrow shown in Fig. 1), whereas during heating this anomaly is masked by the reverse MT. The $M(T)$ data confirm (see below) that it coincides with the para-to-ferromagnetic phase transition in the austenite phase. The characteristic MT temperatures, located in the temperature range of 280–310 K, and the Curie temperature of the austenite phase are summarized in Table I. These temperatures are about 10–20 K lower than the ones observed in the bulk parent alloy,[18] which is related to the influence of structural defects formed during a rapid solidification.[19] Note,

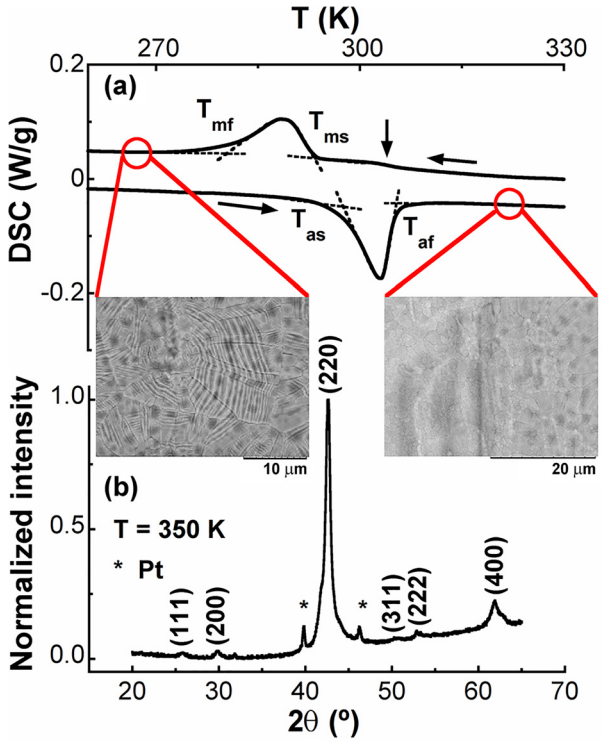

FIG. 1. (a) DSC curves of as-cast Ni-Mn-In ribbon. (b) X-ray diffraction pattern collected at 350 K. Asterisks mark the diffraction peaks corresponding to the Pt heater. Insets: SEM micrographs of the free-side of the ribbon in the austenite (right) and martensite (left).

however, that the thermal hysteresis is similar to other MetaMSMAs.[20,21]

The X-ray powder diffraction pattern of the cubic austenitic phase is shown in Fig. 1(b). The Rietveld analysis indicates a mixture of $L2_1$ (with a volume fraction of 78%) and B2 (22%) crystal structures with cell parameters $a = 6.010$ and 3.001 Å, respectively, consistent with the Ni-Mn-In ribbons of a similar composition.[16,22–24] The insets of Fig. 1 show the SEM images of the ribbon surfaces collected in the martensite and austenite. The samples are well-crystallized with the grains of irregular shapes and broad size distribution between 1 and 10 μm, which is typical for melt-spun ribbons.[25] The left inset (martensite state) shows the twinning structure covering grains according to their in-plane crystallographic orientation.

The heating/cooling thermomagnetization curves under low magnetic field (0.01 T), depicted in the inset of Fig. 2, confirm both MT, by a hysteretic abrupt change of the magnetization, and a Curie point of austenite during cooling. The start (T_{ms}, T_{as}) and finish (T_{mf}, T_{af}) values of the martensitic

TABLE I. Values of the martensite start (T_{ms}) and finish (T_{mf}) temperatures, austenite start (T_{as}) and finish (T_{mf}) temperatures, thermal hysteresis of MT ($\Delta T = T_{af} - T_{ms}$), and Curie temperature of the martensite (T_C^M) and austenite (T_C^A) in $Ni_{50}Mn_{35}In_{15}$ ribbons obtained from the DSC and low-field $M(T)$ measurements.

Measuring method	T_{ms} (K)	T_{mf} (K)	T_{as} (K)	T_{af} (K)	ΔT (K)	T_C^M (K)	T_C^A (K)
DSC	293	279	297	305	12	…	305
Magnetization	293	279	295	304	11	199	309

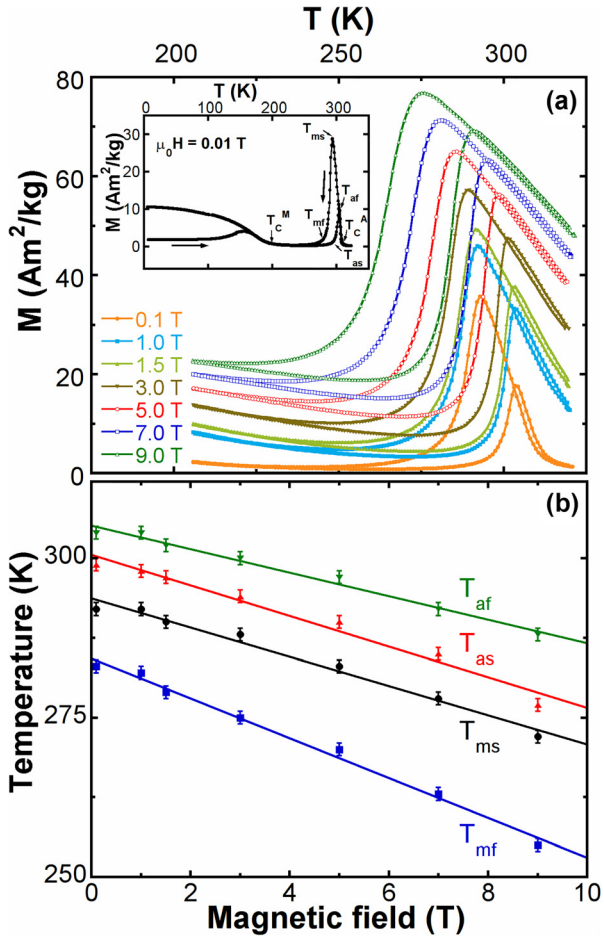

FIG. 2. (a) Temperature dependence of the magnetization under different applied fields. (b) Characteristic martensite temperatures as a function of magnetic field. Inset: ZFC-FC curves under low magnetic field. Arrows indicate heating or cooling pathways.

and austenitic transformation temperatures determined from the $M(T)$ dependences by the tangents method (also used to determine the Curie temperature from magnetization measurements[26]) are consistent with the temperatures estimated from the calorimetric measurements (see Table I). The differences at low temperatures (below 200 K) between the ZFC (zero-field cooling protocol, i.e., the sample was cooled under zero-magnetic field, after which the data were collected on warming under the magnetic field) and FC (field cooling protocol, i.e., the data were acquired on cooling under the magnetic field) curves indicate a heterogeneous magnetic state with the coexistence of antiferromagnetic and ferromagnetic interactions, which has been observed in other MetaMSMAs.[24,27] From a joint analysis of the $M(T)$ and DSC curves, the sequence of phase transitions that the samples undergo on heating is as follows: first, a purely magnetic phase transition in the martensite state occurs at T_C^M. Then, MT occurs from the weakly magnetic martensite to the ferromagnetic austenite. The drop of the magnetization on further heating indicates that a ferromagnetic transition takes place in the austenite state. The Curie temperatures for the martensite and austenite phases are listed in Table I.

$M(T)$ curves under different magnetic fields in Fig. 2(a) show a considerable influence of the magnetic field on the magnetization values in all phases and in MT itself. Magnetic field shifts the MT to lower temperatures and increases the magnetization jump ΔM as it does in the bulk. The dependences of the MT temperatures with the magnetic field, as extracted from the data in Fig. 2(a), are plotted in Fig. 2(b); they exhibit a linear behavior with different dT/dH slopes ranging from −1.85 to −3.12 K/T. This divergence of slopes reflects the magnetic field induced smearing of the transformation path during cooling only, since the field does not affect the thermal hysteresis in the middle of MT.

The temperature dependence of the magnetic entropy change under different magnetic fields is estimated using the data in Fig. 2(a) and the Maxwell relationship. The results are shown in Fig. 3(a). A large negative peak appears around T_C^A, which represents a conventional MCE. It is well known that, in the vicinity of a ferro-to-paramagnetic transition, the magnetic field aligns the magnetic moments leading to a decrease in magnetic entropy. On the contrary, the magnetic entropy change presents a positive peak at MT, which corresponds to a structural transformation accompanied by a change in the magnetic structure. The former implicates a negative magnetic entropy change, $\Delta S_M^{mag} < 0$, whereas the latter involves a positive entropy change, $\Delta S_M^{st} > 0$. Therefore, the magnetic and structural transitions present opposite contributions to the total magnetic entropy change if both transitions are overlapping ($\Delta S_M = \Delta S_M^{st} + \Delta S_M^{mag}$).

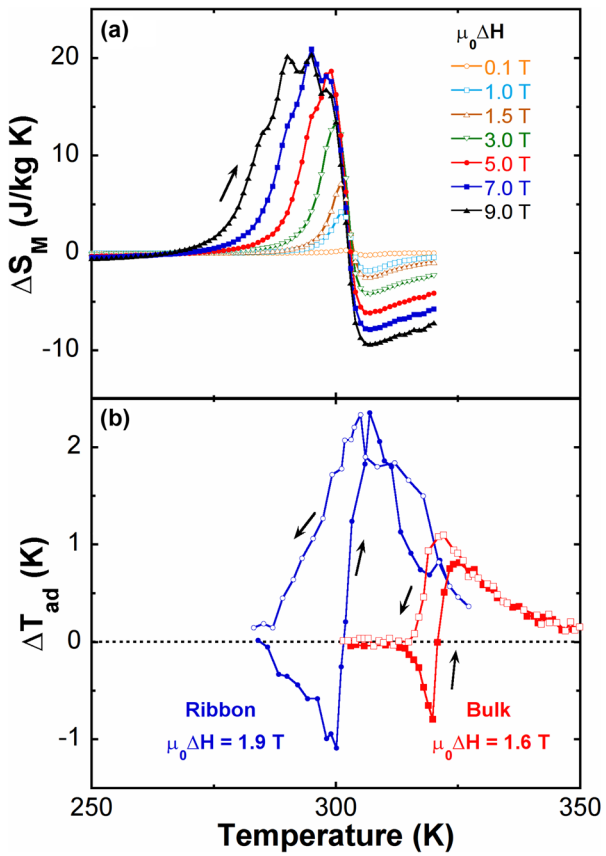

FIG. 3. (a) Magnetic entropy change as a function of the temperature for different applied magnetic fields calculated from thermomagnetization curves. (b) Temperature dependence of the measured adiabatic temperature change for the $Ni_{50}Mn_{35}In_{15}$ ribbon (circles). The data for bulk $Ni_{50}Mn_{35}In_{15}$ (squares), adapted from Ref. 18, are shown for the sake of comparison. Reproduced with permission from Rodionov *et al.* JETP Lett. **101**, 385 (2015). Copyright 2015 Pleiades Publishing, Inc.

The positive value of ΔS_M might indicate a dominant role of the structural contribution at MT. Note that the positive peak moves to lower temperatures under magnetic field as expected from the shift of the MT temperature, whereas the one associated with the second-order ferromagnetic transition moderately moves upwards along temperature axis. The maximum of ΔS_M for both transitions amounts to 20.1 and −9.4 J/kg K (7.0 and −2.5 J/kg K) for 9 T (1.5 T), respectively. These values are similar to the reported ones in the bulks[28,29] and ribbons[24,30] of Ni-Mn-In.

From the dT/dH slopes, the transformation entropy change, ΔS, induced by magnetic field is approximately given by the Clausius–Clapeyron relation:[4] $dH/dT_A \sim \Delta S/\Delta M$, where ΔM is the magnetization difference between the austenite and martensite phases and T_A is the equilibrium temperature of the reverse MT defined as $T_A = (T_{as} + T_{af})/2$. Accepting $\Delta M = 54$ A m^2/kg for a magnetic field change of 9 T at the reverse MT in Fig. 2(a), and $dT_A/dH = -2.2$ K/T, ΔS results in 24.5 J/kg K, which is close to the entropy change calculated from the Maxwell relation. Using the DSC measurements, we have estimated the transformation enthalpy to be equal to $\Delta H^{MT} = 8$ J/g, which corresponds to a total entropy change at MT of $\Delta S^{MT} = 27$ J/kg K. Note that the estimated values of ΔS_M on heating are lower than this. As it is known, ΔS^{MT} is an upper bound of the possible attainable magnetic entropy change; therefore, the reduced values of ΔS_M could be due to the closeness of the magnetic phase transition to MT, bringing a competition between the conventional and inverse MCEs.

The temperature dependences of ΔT_{ad} in the field of 1.9 T are presented in Fig. 3(b). Note that the application of a magnetic field in adiabatic conditions has different consequences in the first and second order phase transitions. On heating across reverse MT, ΔT_{ad} exhibits a negative maximum equal to 1.1 K at $T_A = 300$ K, corresponding to an inverse MCE. The positive magnetic entropy change at the reverse MT (see Fig. 3(a)) involves the negative contribution of the sample lattice under adiabatic conditions, resulting in a decrease in the sample temperature. On further heating, a conventional MCE is observed. In this case, ΔT_{ad} shows positive values with a maximum of 2.3 K at $T = 307$ K corresponding to the second-order ferromagnetic transition. This increase in the sample temperature results from the lattice entropy contribution that is necessary to compensate the magnetic entropy change if the magnetic field is applied adiabatically.

On cooling, the maximum associated with the para-to-ferromagnetic phase transition occurs roughly at the same temperature and reaches an identical value as in the heating run. ΔT_{ad} decreases close to zero in the vicinity of the forward MT. Such discrepancies on the adiabatic temperature change in both cooling and heating sequences have been usually attributed to thermal and magnetic field hysteresis occurring across MT,[31] although recently the role of the latent heat exchange linked with irreversible structural transformations has been analysed.[32] In our case, three obvious factors influencing the value of inverse MCE can be considered as the most important ones: (i) overlapping of MT with T_C^A, (ii) the temperature width of two-phase region during the forward and reverse MT, and (iii) the temperature hysteresis between forward and reverse MT. Reduced value of inverse MCE during heating run results from a compensating influence of the ferromagnetic ordering of austenite and structural transformation [factor (i)], as well as from the relatively high value of T_{af} - $T_{as} = 9$ K and hence reduced volume fraction of martensitic phase that can be transformed into austenite by applied field of 1.9 T (see Table I and Fig. 2(b)). The absence of inverse MCE during cooling is explained by factor (iii) (according to Table I, ΔT is 11–12 K) since it prevents that any portion of martensitic phase formed during cooling to the measuring temperatures below T_{ms} can transform back to austenite under 1.9 T (see Fig. 2(b)). The adiabatic temperature change can be estimated assuming that the heat capacity, C_p, of a material has little dependence on the magnetic field and the adiabatic temperature change can be estimated as $\Delta T = (-T/C_p)\Delta S$.[4] In $Ni_{50}Mn_{35}In_{15}$, the C_p satisfies such condition[31] and could be roughly accepted to be equal to 0.5 J/g K. Thus, $\Delta T = -4.9$ K has been calculated for a magnetic field change of 1.5 T on heating. Disagreement between the theoretical and experimental values has been usually attributed to the non-equilibrium effects,[4] as well as aforementioned factors.

For the sake of comparison, Fig. 3(b) also depicts the ΔT_{ad} data obtained at the field of 1.6 T for the bulk $Ni_{50}Mn_{35}In_{15}$ alloy,[18] which displays inverse and direct MCEs and qualitatively reproduces the temperature dependence of ΔT_{ad} for ribbon. In both cases, the thermal hysteresis of MT and closeness of the first and second-order phase transitions lead to a decrease in MCE, as observed in other MetaMSMAs.[33] The difference between the transition temperatures in the bulk and ribbon could be due to the composition variation and higher density of crystalline defects in ribbons.[34]

It would be expected that, associated with the magnetic field-induced shift of MT to lower temperatures, ΔT_{ad} increases substantially with the magnetic field. Indeed, a study under much higher magnetic fields in $Ni_{50}Mn_{35}In_{15}$ bulk alloy has revealed that the inverse MCE reaches to −7.0 K for $\mu_0\Delta H = 6$ T, but this value does not increase with a further raising of the magnetic field because it is limited by the latent heat of MT.[31]

To conclude, we have fabricated a well-studied $Ni_{50}Mn_{35}In_{15}$ in the form of the ribbon as a model object for a special study of the magnetocaloric effects in the adiabatic measurements for MetaMSMA ribbons. Ribbons present a martensite transformation close to room temperature that is driven downwards almost linearly by the magnetic field. The substantial values of the conventional and inverse magnetocaloric responses have been revealed by the direct adiabatic measurements using a unique in-house made set-up and confirmed by the traditional magnetization method. Determining the adiabatic temperature change in ribbons will help to optimize the magnetic and magnetocaloric properties in the MetaMSMA materials with enhanced heat transfer, which will present direct implications in the development of MR devices.

The financial support from CONACYT Mexico (Project No. CB-2010-01-157541) and the Laboratorio Nacional de Investigaciones en Nanociencias y Nanotecnología (LINAN, IPICyT), and the Spanish Ministry of Economy and

Competitiveness (MAT2014-56116-C4-3-4-R) is acknowledged. We would like to thank the SGIker services for the technical support and would especially like to thank Dr. Iñaki Orue and Aitor Larrañaga.

[1]O. Gutfleisch, M. A. Willard, E. Brück, C. H. Chen, S. G. Sankar, and J. P. Liu, Adv. Mater. **23**, 821 (2011).
[2]V. Franco, J. S. Blázquez, B. Ingale, and A. Conde, Annu. Rev. Mater. Res. **42**, 305 (2012).
[3]A. Smith, C. R. H. Bahl, R. Bjørk, K. Engelbrecht, K. K. Nielsen, and N. Pryds, Adv. Energy Mater. **2**, 1288 (2012).
[4]A. Planes, L. Mañosa, and M. Acet, J. Phys.: Condens. Matter **21**, 233201 (2009).
[5]V. V. Khovaylo, V. V. Rodionova, S. N. Shevyrtalov, and V. Novosad, Phys. Status Solidi B **251**, 2104 (2014).
[6]S. Qian, J. Ling, Y. Hwang, R. Radermacher, and I. Takeuchi, Int. J. Refrig. **56**, 65 (2015).
[7]V. Franco, J. S. Blázquez, and A. Conde, Appl. Phys. Lett. **89**, 222512 (2006).
[8]V. Vega, L. González, J. García, W. O. Rosa, D. Serantes, V. M. Prida, G. Badini, R. Varga, J. J. Suñol, and B. Hernando, J. Appl. Phys. **112**, 33905 (2012).
[9]B. Yu, M. Liu, P. W. Egolf, and A. Kitanovski, Int. J. Refrig. **33**, 1029 (2010).
[10]A. M. Aliev, A. B. Batdalov, I. K. Kamilov, V. V. Koledov, V. G. Shavrov, V. D. Buchelnikov, J. García, V. M. Prida, and B. Hernando, Appl. Phys. Lett. **97**, 212505 (2010).
[11]J. Y. Law, V. Franco, and R. V. Ramanujan, J. Appl. Phys. **110**, 23907 (2011).
[12]A. Waske, H. Hermann, N. Mattern, K. Skokov, O. Gutfleisch, and J. Eckert, J. Appl. Phys. **112**, 123918 (2012).
[13]B. Schwarz, N. Mattern, J. D. Moore, K. P. Skokov, O. Gutfleisch, and J. Eckert, J. Magn. Magn. Mater. **323**, 1782 (2011).
[14]ASTM International, *Standard Test Method for Determination of Transformation Temperature of Nickel-Titanium Shape Memory Alloys by Bend and Free Recovery* (ASTM International, West Conshohocken, PA, 2010).
[15]J. Rodríguez-Carvajal, Phys. B: Condens. Matter **192**, 55 (1993).
[16]A. K. Pathak, M. Khan, I. Dubenko, S. Stadler, and N. Ali, Appl. Phys. Lett. **90**, 262504 (2007).
[17]P. Álvarez-Alonso, J. López-García, G. Daniel-Perez, D. Salazar, P. Lázpita, J. P. Camarillo, H. Flores-Zuñiga, D. Rios-Jara, J. L. Sánchez-Llamazares, and V. A. Chernenko, Key Eng. Mater. **644**, 215 (2015).
[18]I. D. Rodionov, Y. S. Koshkid'ko, J. Cwik, A. Quetz, S. Pandey, A. Aryal, I. S. Dubenko, S. Stadler, N. Ali, I. S. Titov, M. Blinov, M. V. Prudnikova, V. N. Prudnikov, E. Lähderanta, and A. B. Granovskii, JETP Lett. **101**, 385 (2015).
[19]V. A. Chernenko, E. Cesari, J. Pons, and C. Segui, J. Mater. Res. **15**, 1496 (2000).
[20]T. Krenke, E. Duman, M. Acet, E. Wassermann, X. Moya, L. Mañosa, A. Planes, E. Suard, and B. Ouladdiaf, Phys. Rev. B **75**, 104414 (2007).
[21]J. D. Santos, T. Sanchez, P. Alvarez, M. L. Sanchez, J. L. Sánchez Llamazares, B. Hernando, L. Escoda, J. J. Suñol, and R. Varga, J. Appl. Phys. **103**, 07B326 (2008).
[22]J. L. Sánchez Llamazares, T. Sanchez, J. D. Santos, M. J. Pérez, M. L. Sanchez, B. Hernando, L. Escoda, J. J. Suñol, and R. Varga, Appl. Phys. Lett. **92**, 12513 (2008).
[23]J. L. Sánchez Llamazares, B. Hernando, C. García, J. González, L. Escoda, and J. J. Suñol, J. Phys. Appl. Phys. **42**, 45002 (2009).
[24]X. G. Zhao, C. C. Hsieh, J. H. Lai, X. J. Cheng, W. C. Chang, W. B. Cui, W. Liu, and Z. D. Zhang, Scr. Mater. **63**, 250 (2010).
[25]P. J. Ibarra-Gaytan, C. F. Sánchez-Valdes, J. L. S. Llamazares, P. Álvarez-Alonso, P. Gorria, and J. A. Blanco, Appl. Phys. Lett. **103**, 152401 (2013).
[26]E. Petrovský and A. Kapička, J. Geophys. Res.: Solid Earth **111**, B12S27, doi:10.1029/2006JB004507 (2006).
[27]M. Acet and E. F. Wassermann, Adv. Eng. Mater. **14**, 523 (2012).
[28]Z. D. Han, D. H. Wang, C. L. Zhang, S. L. Tang, B. X. Gu, and Y. W. Du, Appl. Phys. Lett. **89**, 182507 (2006).
[29]J.-H. Chen, N. M. Bruno, I. Karaman, Y. Huang, J. Li, and J. H. Ross, J. Appl. Phys. **116**, 203901 (2014).
[30]B. Hernando, J. L. Sánchez Llamazares, V. M. Prida, D. Baldomir, D. Serantes, M. Ilyn, and J. González, Appl. Phys. Lett. **94**, 222502 (2009).
[31]M. G. Zavareh, C. S. Mejía, A. K. Nayak, Y. Skourski, J. Wosnitza, C. Felser, and M. Nicklas, Appl. Phys. Lett. **106**, 71904 (2015).
[32]M. Ghahremani, H. ElBidweihy, L. H. Bennett, E. Della Torre, M. Zou, and F. Johnson, J. Appl. Phys. **113**, 17A943 (2013).
[33]V. V. Khovaylo, K. P. Skokov, O. Gutfleisch, H. Miki, R. Kainuma, and T. Kanomata, Appl. Phys. Lett. **97**, 52503 (2010).
[34]J. Liu, N. Scheerbaum, J. Lyubina, and O. Gutfleisch, Appl. Phys. Lett. **93**, 102512 (2008).